WSRC-MS-96-0590

CONF-970726-- 16

Power Distribution for an Am/Cm Bushing Melter

by

C. Gong

Westinghouse Savannah River Company
Savannah River Site
Aiken, South Carolina 29808

B. J. Hardy

A document prepared for 1997 ASME PRESSURE VESSEL AND PIPING CONFERENCE at Orlando, FL, USA from 7/27/97 - 7/31/97.

DOE Contract No. **DE-AC09-89SR18035 & DE-AC09-96SR18500**

DISCLAIMER

POWER DISTRIBUTION FOR AN AM/CM BUSHING MELTER

Chung Gong
Savannah River Technology Center
Westinghouse Savannah River Company
773-42A, Room 154
Aiken, South Carolina 29808

Telephone: (803) 725-3167
Fax: (803) 725-8829
e-mail: chung.gong@srs.gov

Bruce J. Hardy
Savannah River Technology Center
Westinghouse Savannah River Company
704-1T, Room 232
Aiken, South Carolina 29808

Telephone: (803) 557-7113
Fax: (803) 557-7008
e-mail: bruce.hardy@srs.gov

Decades of nuclear material production at the Savannah River Site (SRS) has resulted in the generation of large quantities of the isotopes Am^{243} and Cm^{244}. Currently, the Am and Cm isotopes are stored as a nitric acid solution in a tank. The Am and Cm isotopes have great commercial value but must be transferred to the Oak Ridge National Laboratory (ORNL) for processing. The nitric acid solution contains other isotopes and is intensely radioactive, which makes storage a problem and precludes shipment in the liquid form. In order to stabilize the material for onsite storage and to permit transport the material from SRS to ORNL, it has been proposed that the Am and Cm be separated from other isotopes in the solution and vitrified.

Vitrification will be effected by depositing a liquid feed stream containing the isotopes in solution, together with a stream of glass frit, onto the top of a molten glass pool in a melter. The glass is non-conducting and the melter is a Platinum/Rhodium alloy vessel which is heated by passing an electric current through it. Because most of the power is required to evaporate the liquid feed at the top of the glass pool, power demands differ for the upper and lower parts of the melter. In addition, the melter is batch fed so that the local power requirements vary with time. In order to design a unique split power supply, which ensures adequate local power delivery, an analysis of the melter power distribution was performed with the ABAQUS finite element code. ABAQUS was used to calculate the electric potential and current density distributions in the melter for a variety of current and potential boundary conditions. The results of the calculation were compared with test data and will be used to compute power densities for input to a computational fluid dynamics model for the melter.

POWER DISTRIBUTION FOR AN AM/CM BUSHING MELTER

Chung Gong
Savannah River Technology Center
Westinghouse Savannah River Company
773-42A, Room 154
Aiken, South Carolina 29808

Bruce J. Hardy
Savannah River Technology Center
Westinghouse Savannah River Company
704-1T, Room 232
Aiken, South Carolina 29808

1. INTRODUCTION

Decades of nuclear material production at the Savannah River Site (SRS) has resulted in the generation of kilogram quantities of the isotopes Am^{243} and Cm^{244}. Currently, the Am and Cm isotopes are stored in a tank as a nitric acid solution. The solution contains other isotopes and is intensely radioactive, which makes long term storage a problem and precludes shipment in the liquid form. The Am and Cm isotopes are not merely waste material, the isotopes have great commercial value but must be transferred to the Oak Ridge National Laboratory (ORNL) for processing. In order to stabilize the material for onsite storage and to transport the material from SRS to ORNL, it has been proposed that the Am and Cm be separated from the majority of the other isotopes in the solution and vitrified.

Vitrification will be effected by depositing a liquid feed stream containing the isotopes in solution, together with a stream of glass frit, onto the top of a molten glass pool in a melter. The glass is non-conducting and the melter is a rectangular vessel composed of platinum/rhodium alloy and which is resistively heated. The majority of the evaporation of water in the liquid feed occurs in the frit bed formed on the surface of the glass pool. The wetted frit bed is called a "cold cap". Because most of the power is required to evaporate the liquid, power demands differ for the upper and lower parts of the melter. In addition, the melter is batch fed so that the power requirements at the top and bottom of the melter vary with time. To vary the fraction of the total power delivered to the upper and lower parts of the melter, pairs of upper and lower electrodes were placed on the melter and connected to variable power supplies.

In order to ensure that the electrode configuration could effectively vary power between the top and bottom of the melter, and to identify regions of high power density, an analysis of the melter power distribution was performed with the ABAQUS® finite element code. ABAQUS was used to calculate the electric potential and current density distributions in the

melter for a variety of current and potential boundary conditions. The results of the calculation were compared with test data and were used to compute power densities for input to a computational fluid dynamics model for the melter.

During melter heat-up, thermal expansion may cause permanent deformation. Further, the melter will operate at temperatures near 1400°C. At these temperatures the melter is entirely in the regime of plastic deformation and the structural integrity and stability of the melter was questioned. The stress and strain in the melter during heat-up and at the operating temperature was estimated from a model based on the ABAQUS code .

This report documents the power distribution and stress calculations performed for Melters 2A and 2B which are to be used in the Am/Cm vitrification program.

2. BACKGROUND

The design of Melters 2A and 2B, is based on operating experience with Melter 1. Melter 1 was a rectangular box with a bottom which sloped toward a central drain tube. Melter 1 was approximately 11 in. tall, 10 in. wide and 2.5 in. deep. The top of the melter had a 2.5 in. by 10 in. rectangular opening. One pair of electrodes was attached on opposite sides of the melter.

Initially, it was believed that Melter 1 could be run as a continuous process. However, operating experience dictated that it was necessary to run in batch mode. During tests with Melter 1, it soon became obvious that the operation of the melter must be divided into three phases; feeding, heating and a pouring. In the feeding phase, inventory is accumulated by depositing nitric acid solution and glass frit on the surface of the glass pool. The majority of the power is used to evaporate the nitric acid solution. Therefore, most of the power must be applied to the top of the melter during the feeding phase . After sufficient inventory is accumulated in the melter, the heating phase begins. In this phase the feed is stopped and the remaining liquid evaporates from the cold cap. The remaining layer of dried frit and crust is heated until it is melted into the glass pool, which is heated until an equilibrium state is reached within the melter. It is believed that the melter may be allowed to idle indefinitely at this state without adversely affecting the product or system. During the heating phase it is believed that it will be necessary to shift power toward the bottom of the melter. After equilibrium has been reached in the heating phase, the glass is ready to pour. This is the pouring phase. Glass pour is initiated by melting the solid glass in the

drain tube with the drain tube heater. It is believed that the power distribution during the pouring phase will need to be uniform or shifted slightly toward the bottom of the melter.

In the Melter 1 tests it was found that radiative losses from the top were sufficiently high that the glass in this region was not completely melted when the plenum was in place. Because of this behavior, Melters 2A and 2B were designed with a partially covered top to direct thermal radiation onto the cold cap rather than allowing it to escape into the plenum. In addition, two pairs of electrodes were attached to Melters 2A and 2B and connected to variable power supplies. The pairs of electrodes are attached to the narrow sides of the melters at the top and bottom, see Figures 1-1 and 1-2. This electrode geometry allows the power to be varied between the top and bottom of the melter as needed for the particular phase of operation.

Excessive thermally induced strain was also a problem with Melter 1. Melter 1 was encased in cast refractory with no allowance for thermal expansion. Further, both the top and bottom of Melter 1 were rigidly fixed, allowing for no vertical expansion. When the melter was heated it expanded against the refractory material, which had a substantially lower coefficient of thermal expansion. In addition, the melter expanded against the rigid top and bottom members. The walls of Melter 1 experienced substantial buckling and a tear was observed. It must be noted however, that the tear may have occurred during attempts to force glassy deposits into the glass pool by pushing against them with a mullite rod. In order to allow for vertical thermal expansion in Melters 2A and 2B, the bottom of the melter was supported on springs. Lateral expansion against the refractory material was accommodated by using fiberfrax (ceramic papers) as a spacer.

3. MELTER GEOMETRY

Melters 2A and 2B are flat, tall rectangular boxes made of platinum-rhodium alloys and were fabricated by GAFtech, Inc. of Nashville, TN. Because differences in the melter configurations are insignificant with regards to power and stress distributions, only one melter model was used for both Melters 2A and 2B . The height of both melters is 11 inches, the width is 10 inches and the depth is 2.75 inches, see Figures 1-1 and 1-2.

There are two pairs of flat electrodes, referred to as "ears", on the narrow sides of the melter. One pair of ears primarily delivers power to the upper part of the melter while the other pair of ears primarily supplies power to the bottom. Inside the melter there are two

pairs of vertical screens welded to the narrow side walls with the longitudinal axis of the screens traversing the width of the melter. In order to relieve thermal buckling stresses, each of the screens has a cusp like bend at approximately one inch from each end. Additionally, two cross braces (in the form of an X) are attached between the two top screens at a distance of three inches from ends. The middle screens are also cross braced. A flange plate is attached at the top of the melter. The melter is constructed with 0.06 inches thick platinum-rhodium alloys plates except the top flange (including the drain wall) which are made of 0.03 inch thick plates. The ears are 0.188 inches thick.

4. NUMERICAL METHODS

4.1. Method of Analysis

The finite element method was used to numerically model the electrical and mechanical behavior of Melters 2A and 2B. The mesh was generated with the pre-processor, MSC/PATRAN® and the analysis was performed with the ABAQUS® code. The ABAQUS POST post-processor was used to facilitate the post-processing of the results.

4.2. Description of the Pre- and Post-processor

MSC/PATRAN® [MSC/PATRAN, 1996] is a versatile geometric and graphic modeling code developed by PDA Engineering which was acquired by the MacNeal-Schwendler Corporation. The MSC/PATRAN system's ability to interface with a large array of applications is provided by the PATRAN Neutral File, the PATRAN Results File, and the Application Interface. Post-processing of the results was accomplished using ABAQUS POST.

4.3. Main Processor

ABAQUS® [ABAQUS, 1995], is a general purpose finite element analysis program with special emphasis on advanced linear and nonlinear structural engineering, heat transfer as well as coupled thermal-electrical applications. Hibbitt, Karlsson & Sorensen, Inc. (HKS) developed and support this computer code. The ABAQUS version presently in use at SRS (5.5-1N) is marketed by HKS as a "Nuclear QA Grade" code that complies with the NQA-1 quality assurance standard. Details of the Quality Assurance controls for the ABAQUS code may be found in the Technical and QA Plan for ABAQUS.

4.4. Finite Element Modeling

Melters 2A and 2B possess symmetry with respect to two orthogonal planes. In the case of symmetrically applied loads arising from a uniform temperature distribution, a quarter model cut out along the symmetry planes of the melter was sufficient for the analysis. However, in the analysis of the power distribution, the electrical currents flow from the ears on one side of the melter to those on the other side. The current density distribution then reduces the problem to reflective symmetry about the plane through the long cross-section of the melter which contains the four ears.

For the power distribution analysis, ABAQUS requires solid continuum elements in the model. This model will also be used for thermal stress analysis. The melter is constructed with thin plates.

The thinnest plate in the melter is only 0.03 inches thick. In order to maintain a mathematically tolerable aspect ratio, the other dimensions of the elements were less than 0.12 inches (for double elements in the thickness of the plate) so that the aspect ratio was kept below 8. Attempts to maintain a low aspect ratio in the model resulted in an excessive increase in the number of elements. However, through several trial runs, a workable finite element model was developed The average aspect ratio of the elements in the melter was 7.35. Whereas in the top flange, the aspect ratios were higher than 8, and the maximum aspect ratio reached 32. At the normal intersections of the melter plates and screens the elements became smaller. In these dense regions the aspect ratios of the elements were on the order of 56. The total number of solid continuum elements in this model was 12,568 with 20,428 nodes (total number of variables is 40,856).

There were twelve circular holes on each of the top screens. Two sets of double cross-bars were installed to connect each pair of the top and middle screens. The cusps on both ends of each of the screens were also modeled.

The melter was meshed with 3-D solid continuum elements DC3D8E (8-node linear brick) in the coupled thermal-electrical analysis with ABAQUS. In a small transition region where the geometry precludes the use of DC3D8E, twelve DC3D6E (6-node linear triangular prism) elements were implemented.

5. MATERIAL PROPERTIES

Melters 2A and 2B are to be manufactured with platinum-rhodium alloys. Two compositions have been chosen as the primary materials for the melter: 90% platinum 10% rhodium alloy and 80% platinum 20% rhodium alloy.

There is a paucity of material data for platinum-rhodium alloys at the operating temperatures for the melter. The temperature dependent properties of platinum-rhodium alloys are not readily available from usual material handbooks. Material properties of the platinum-rhodium alloys in this study were mostly obtained from two sources, viz., a reference book [Vines, 1941] published by the International Nickel Company and scattered pieces of information obtained from Dr. Louis Toth of Engelhard-Clal [Toth, 1996], who assisted us with our literature search. Many of the high temperature physical properties of the platinum-rhodium alloys were selectively chosen from conflicting data or extrapolated from the limited data available. All the material properties data obtained are converted into the SI system, which constitutes the system of units for this analysis.

5.1. Mass Density

The mass density of the platinum rhodium alloys can be found in References [Toth, 1996, ASM, 1990]. The values listed in Table 5-1 are the mass densities of the alloys at 30°C [ASM, 1990, p. 710, Table 8].

Table 5-1. Mass density of platinum-rhodium alloys

Alloy	Density (kg/m^3)
90% Pt - 10% Rh	19,970
80% Pt - 20% Rh	18,740

5.2. Thermal Conductivity

In view of the fact that platinum-rhodium alloys are used extensively for high temperature applications, it is somewhat surprising that the thermal properties of platinum-rhodium alloys are particularly scarce. Insofar as the authors could discern, the specific heat data for the alloys are simply not available. Only a few experimentally obtained values for thermal conductivity could be found for two different of platinum rhodium alloys, namely, 87% platinum 13% rhodium and the 60% platinum-40% rhodium. Test data for the 87% platinum-13% rhodium alloy was fitted with least squares into a simple formula [Mølgaard, 1968]:

$$K_{PR} = 60.7 - 9.2\,(10^3/T) \qquad (5\text{-}1)$$

where: K_{PR} = thermal conductivity of the 87% platinum-13% rhodium alloy in W / K m
T = temperature in K.

The test data for the 60% platinum-40% rhodium alloy was provided by Dr. Louis Toth [Toth, 1996]. The thermal conductivity as a function of temperature is listed in Table 5-2.

Table 5-2. Thermal conductivity of the 60% platinum 40% rhodium alloy

Temperature K	Temperature °C	Thermal Conductivity Cal/sec/cm/K	Thermal Conductivity Watt/M K
250	-23.15	0.105	43.97
400	126.85	0.120	50.25
600	326.85	0.140	58.63
800	526.85	0.155	64.91
1000	726.85	0.165	69.10
1200	926.85	0.172	72.03
1400	1126.85	0.180	75.38
1600	1326.85	0.182	76.21
1800	1526.85	0.187	78.31

5.3. Thermal Expansion Coefficients

The linear thermal expansion ratios (i.e., the ratio of the expanded length to the undeformed length, (L_t / L_o)) were provided by Dr. Toth [Toth, 1996, Table VIII]. The coefficients of thermal expansion were then computed from the linear thermal expansion ratios as listed in Table 5-3.

Table 5-3. The Coefficients of Thermal Expansion for Platinum Rhodium Alloys

Temperature °C	Thermal Expansion Coefficient			
	Pt (90%)-Rh(10%)		Pt (80%)-Rh(20%)	
	L_t/L_o- 1.0	Strain/K	L_t/L_o- 1.0	Strain/K
0	0	0.00000000E+00	0	0.00000000E+00
100	0.001	1.00000000E-05	0.00063	6.30000000E-06
200	0.002	1.00000000E-05	0.0014	7.00000000E-06
300	0.003	1.00000000E-05	0.0023	7.66666667E-06
400	0.0041	1.02500000E-05	0.0032	8.00000000E-06
500	0.0051	1.02000000E-05	0.0043	8.60000000E-06
600	0.0061	1.01666667E-05	0.0053	8.83333333E-06
700	0.0072	1.02857143E-05	0.0063	9.00000000E-06
800	0.0083	1.03750000E-05	0.0075	9.37500000E-06
900	0.0094	1.04444444E-05	0.0087	9.66666667E-06
1000	0.0106	1.06000000E-05	0.0099	9.90000000E-06
1100	0.0117	1.06363636E-05	0.0112	1.01818182E-05
1200	0.0131	1.09166667E-05	0.0125	1.04166667E-05
1300	0.0144	1.10769231E-05	0.0138	1.06153846E-05
1400	0.0158	1.12857143E-05	0.0152	1.08571429E-05
1500	0.0176	1.17333333E-05	0.0167	1.11333333E-05

5.4. Electrical Conductivity

If the temperature is not extremely low, the Wiedemann-Franz law states that for a metal, the ratio of the thermal conductivity to the electrical conductivity is directly proportional to the temperature. Further, the value of the proportionality constant is independent of the particular metal [Kittel, 1966]. The electrical conductivities of the 90% platinum 10% rhodium and 87% platinum 13% rhodium alloys are derived from the resistivity listed in Table 39 of [Vines, 1941, page 89]. With both thermal conductivity and electrical conductivity computed from the experimental data, the Lorenz number defined by the Wiedemann-Franz law can be obtained. The derived temperature dependent electrical conductivity of the platinum-rhodium alloys are listed in Table 5-4.

Table 5-4. The Electrical Conductivity of the Platinum Rhodium Alloys

Temperature °C	Electrical Conductivity (1/ohm-Meter)	
	90% Platinum 10% Rhodium	87% Platinum 13% Rhodium
0.0	5.434783E+06	5.263158E+06
100.0	4.661049E+06	4.552905E+06
200.0	4.086303E+06	4.023821E+06
300.0	3.647505E+06	3.614806E+06
400.0	3.301812E+06	3.287419E+06
500.0	3.022682E+06	3.017866E+06
600.0	2.791362E+06	2.792126E+06
700.0	2.596647E+06	2.601660E+06
800.0	2.432759E+06	2.440036E+06
900.0	2.293157E+06	2.301337E+06
1000.0	2.171307E+06	2.180264E+06
1100.0	2.064103E+06	2.073742E+06
1200.0	1.968411E+06	1.978631E+06
1300.0	1.882502E+06	1.893222E+06
1400.0	1.804976E+06	1.816135E+06
1500.0	1.734690E+06	1.746237E+06

6. MODEL DESCRIPTION

This study covers three major fields of physics, namely, heat transfer, electrical conduction and continuum mechanics. The three fields are coupled in this analysis. The effect of temperature in all the properties of the materials is conspicuously appreciable in testing, for instance, the Thomson effect [Jones, 1956] that shows the coupling of thermal and electrical currents in power distribution. Whereas the other factors, such as electrical potential gradients, deformation of the element (the Bardeen and Shockley effect), etc. may also alter the properties of the medium. But the changes in material properties due to factors other than temperature are not significant in this analysis.

6.1. Power Distribution

The power distribution in the melter was calculated with the coupled thermal-electrical analysis model in the ABAQUS code, which exploits the fact that Fourier's law for heat conduction is mathematically identical to the microscopic form of Ohm's law.

In the actual melter, the power supply utilizes a 60 cycle alternating current which is applied across the ears of the melter. The fraction of the total current delivered to the top and

bottom ears is based on the power demands during the particular phase of melter operation. Resistance heating occurs as the current flows through the platinum-rhodium alloy comprising the body of the melter. Because the ABAQUS code can only provide calculations for direct current, the numerical model of the power distribution describes a DC power source operating at the RMS power of the actual AC power supply. At the frequency of the actual AC power supply, it is believed that the DC model will provide an accurate estimate of the actual AC power distribution.

The ABAQUS calculations give the current density vector and the electric potential in the melter shell. The power density is obtained from the simple relation

$$q''' = -\frac{1}{\rho}\,\mathbf{j}\cdot\nabla\phi \qquad (6\text{-}1)$$

where: q''' = power density
$\mathbf{j}$ = current density vector
ρ = electrical resistivity
ϕ = electric potential.

Because the glass and insulation are non-conducting, the current and/or electric potential are used to specify boundary conditions at the ears. For the calculations discussed in this paper, the electric current was used as the boundary condition on the melter ears. The external circuitry required that current entering an upper ear exited from an upper ear and current entering a lower ear exited from a lower ear. Power variation between the upper and lower parts of the melter was effected by changing the fraction of the total current applied to the upper and lower ears. The total current applied to the model for Melters 2A and 2B were based on the RMS power demands and the potential drop for Melter 1, which were 13.5 kW and 3.5 volts, respectively. From the Melter 1 data

$$i = \frac{P}{v} = \frac{13.5\times10^{3}\,W}{3.5\,volts} = 3857.1429 \text{ amps} \qquad (6\text{-}2)$$

where: i = current in amps
P = power in Watts
v = potential drop in volts.

Because, as discussed previously, plane symmetry was invoked for the power distribution model, the total applied current is halved. The total current is thus 1928.5715 amps.

It must be noted that the geometry of Melter 1 differed significantly from that of Melters 2A and 2B. Further, Melter 1 only had one pair of ears. The difference in geometry and in the points of entry change the melter resistance and the current paths through the melter. Therefore, if the same current is applied across Melter 1 and across Melters 2A and 2B, different potential drops and correspondingly different total powers will be obtained. Fortunately, for a fixed division of current between the upper and lower ears, the local power varies linearly with the total power. Hence, the scale factor used to obtain the correct total power can be used to obtain the corrected local powers. Scaling to obtain the correct local power will be particularly important for thermal models which will utilize the power densities from the ABAQUS model as input.

The material used for this model was the 90% platinum 10% rhodium alloy, the temperature dependent electrical properties of which were discussed in a previous section. Because the melter is filled with molten glass at approximately 1450°C the platinum-rhodium alloy was assumed to be at this temperature for the calculations in this report. However, the power distributions obtained from the ABAQUS calculations will be used in detailed heat transfer calculations. The resulting melter temperature profile will be applied to the resistivity and the distribution of the power density will be recalculated. If significant differences are noted, the heat transfer calculations will be repeated and the melter temperature distribution used to determine new electrical resistivities. This process will be repeated until the difference in the power distribution is deemed sufficiently small.

In order to examine the ability to distribute power between the top and bottom of the melter, two current and potential boundary conditions were applied to the ears.

Case 1. 70% of the total current enters the top left ear and exits the top right ear. 30% of the total current enters the bottom left ear and exits the bottom right ear. The clamp on the upper ear is to be located at the bottom of the ear.

Case 2. 100% of the current enters the top left ear and exits the top right ear. The current entering the bottom left ear and exiting the bottom right ear is set to zero. The clamp on the upper ear is to be located at the bottom of the ear.

The current in the lower ears is to be controlled by a saturable core reactor. If the reactor were to lose power, the only resistance to current flow in the external circuit for the lower ears would be the loop impedance. The loop impedance is much lower than that across the melter. Therefore, if all the current were sent to the upper ears and the reactor in the lower circuit lost power, the path of least resistance would be from the top ear to the adjacent bottom ear through the lower current loop into the bottom ear on the opposite side of the melter and out through the top ear of the melter. The transmission of the total current through the melter body between the top and bottom ears might result in excessive heating and burn through. The power density for this accident scenario was calculated by considering another case.

Case 3. 100% of the total current enters the top left ear. The bottom ears were connected by loop of low resistance.

7. RESULTS AND CONCLUSIONS

7.1. Power Distribution Analysis

The current density and potential distributions for Cases 1 and 2 are shown in Figures 7-1 ~ 7-4 and the power distribution, calculated from Eq. 6-2 is shown in Figures 7-5 ~ 7-8. The magnitude of current density heaves around the ears of current incidence and exit, in both cases considered. The current density magnitude is significantly high at the junctions of the screens and the narrow side walls. The maximum and minimum values of the current density magnitudes in Case 1 and 2 may show an order of magnitude apart, however, overall the current density magnitude is about 4.0E+06 amps per square meter in the melter. Further the contours show that the electrical potential (Figure 7-3 and 7-4) and the current density vector (Figures 7-9 and 7-10) are symmetrical about the midplane of the melter. The electrical potential distribution (Figure 7-3) in the case of 70-30% current split is almost parallel to the vertical edges of the melter. It connotes that with the 70-30% current split, the electrical power distribution in the melter is also uniform in the vertical direction.

In the whole melter plots (Figure 7-5 and 7-6), the detail of electrical power density distribution is not perceptible. The distributions of the electrical energy dissipated in the power ears are different in the two cases. The energy dissipated in Case 1 (with 70% of current on the top ears and 30% on the bottom ears) is slightly lower than that in the second

case (with 100% of current on the top ears and no current on the bottom ears). The energy density distribution in the large side plate alone (in Figures 7-7 and 7-8) provides better resolution. The distribution of the dissipated energy in the first case (Figure 7-7) is essentially uniform and the average value is about 7.0E+06 joules per cubic meter. In the second case (with 100% of current on the top ears and no current on the bottom ears), the energy dissipated in the vicinities of the top power ears is about an order of magnitude higher than that in the bottom third of the plate. The energy dissipated in the top ear area is about 1.85E+07 joules per cubic meter. In the region between the top ears, the average energy dissipated is in the neighborhood of 8.8E+06 joules per cubic meter. For the bottom one third of the plate the mean value of the dissipated energy is only 3.0E+06 joules per cubic meter.

From the plots of the current density vector in Figures 7-9 and 7-10, it can be seen that the current enters through the left ear, fans out across the back of the melter, then contracts to flow out the right ear. These figures also show the obvious effect of input current distribution. In the 70-30% split case, the major component (along the width of the melter, axis 2 in the model) of the current density vector spreads evenly over the large plate. Whereas in the case with all the input current concentrated on the top left ear, the major component of the current density vector flows mostly over the top two third of the large plate. Nevertheless, except along the left and right edges, the current density difference between the top and bottom parts of the large plate is less than twofold.

By changing the distribution of input current between the top and bottom power ears, we can effectively control the power distribution in the melter. In this analysis, the influence of the molten frit and the liquid feed is not considered. However, in a steady state, the power supply from the ears will determine the temperature distribution in the melter. The variation due to the motion of the glass and liquid feed is rather transient.

The results obtained in Case 3, confirms the conjecture that the current input into the left top ear will transmit down through the attached low resistance wire which connects the two bottom power ears. The current density contour indicates that the path of least resistance is from the top ear to the adjacent bottom ear through the lower current loop into the bottom ear on the opposite side of the melter and out through the top ear of the melter. The transmission of the total current through the melter body between the top and bottom ears might result in excessive heating and burn through.

This thermal-electrical analysis, in essence, provides vital parametric studies and simulations needed for the temperature-power control of the vitrification process.

The input and result files are saved in the Cray Data Archive. The files are in the directors: /archive/y6749/noscreen3.

REFERENCES

ABAQUS® (version 5.5-1N), 1995, *ABAQUS Theory Manual,* Hibbitt, Karlsson & Sorensen, Inc. 1080 Main Street, Pawtucket, RI 02860-4847.

APGreen, 1992, KAST-O-LITE® 30, A. P. Green, Industries, Inc., Mexico, Missouri, 65265, Tel., 314-473-3626, Fax, 314-473-3330.

ASM, 1990, *Metals Handbook,* tenth edition, volume 2, ASM International Handbook Committee.

Jones, H., 1956, "Theory of Electrical and Thermal Conductivity in Metals", in *Handbuch der Physik* (*Encyclopedia of Physics*), vol. XIX, *Electrical Conductivity I*, Edited by S. Flügge, Springer-Verlag, Berlin.

Kittel, C., 1966, *Introduction to Solid State Physics*, Third edition, John Wiley & Sons, Inc., New York.

Mølgaard, J., and Smeltzer, W. W., 1968, "The thermal conductivity of 87% platinum - 13% rhodium alloy", Short Communications, *Journal of the Less-Common Metals, 16* (1968) pp. 275~278.

MSC/PATRAN® (version 5.0), 1996, *Installation & Operations Manual,* The MacNeal-Schwendler Corporation, 815 Colorado Boulevard, Los Angeles, CA 90041.

Özisik, M. N., 1985, *HEAT TRANSFER, A Basic Approach,* McGraw-Hill Book Company, New York.

Papadakis, E. P., Fowler, K. A., Lynnworth, L. C., Robertson, A., and Zysk, E. D., 1974, "Ultrasonic measurements of Young's modulus and extensional wave attenuation in refractory metal wires at elevated temperatures with application to ultrasonic thermometry", *Journal of Applied Physics,* Vol. 45, No. 6, June 1974. pp. 2409~2420.

Toth, Louis, 1996, *Private communications* ENGELHARD-CLAL, LP, 700 Blair Road, Carteret, New Jersey 07008, Telephone (908) 205-5870, Fax phone (908) 205-7476.

Vines R. F., 1941, *The Platinum Metals and Their Alloys,* Edited by E. M. Wise, The International Nickel Company, Inc., New York.

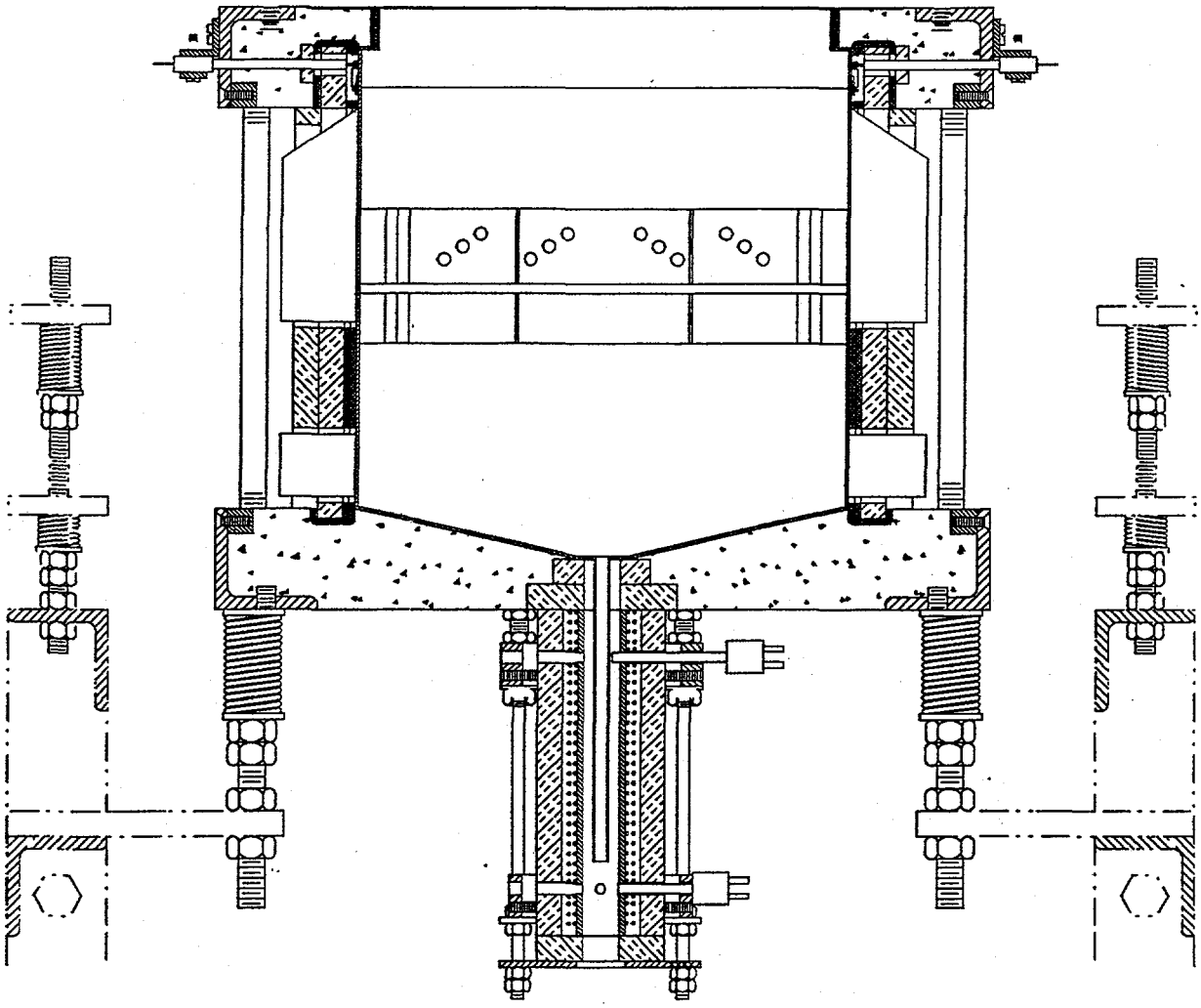

Figure 1-1. Americium/Curium Vitrification Bushing Melter 2A
Middle Plane Section View

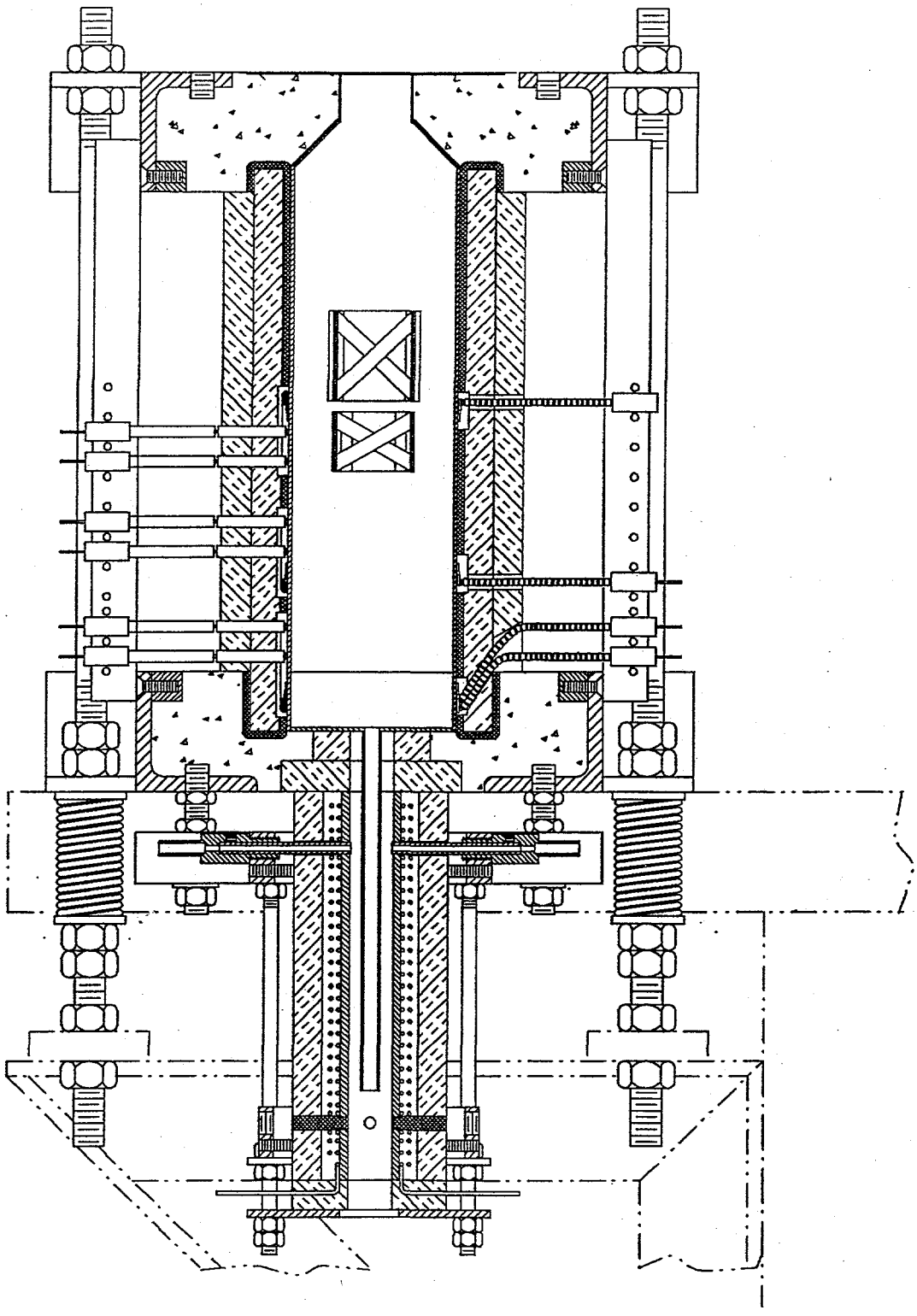

Figure 1-2. Americium/Curium Vitrification Bushing Melter 2A
Side Plane Section View

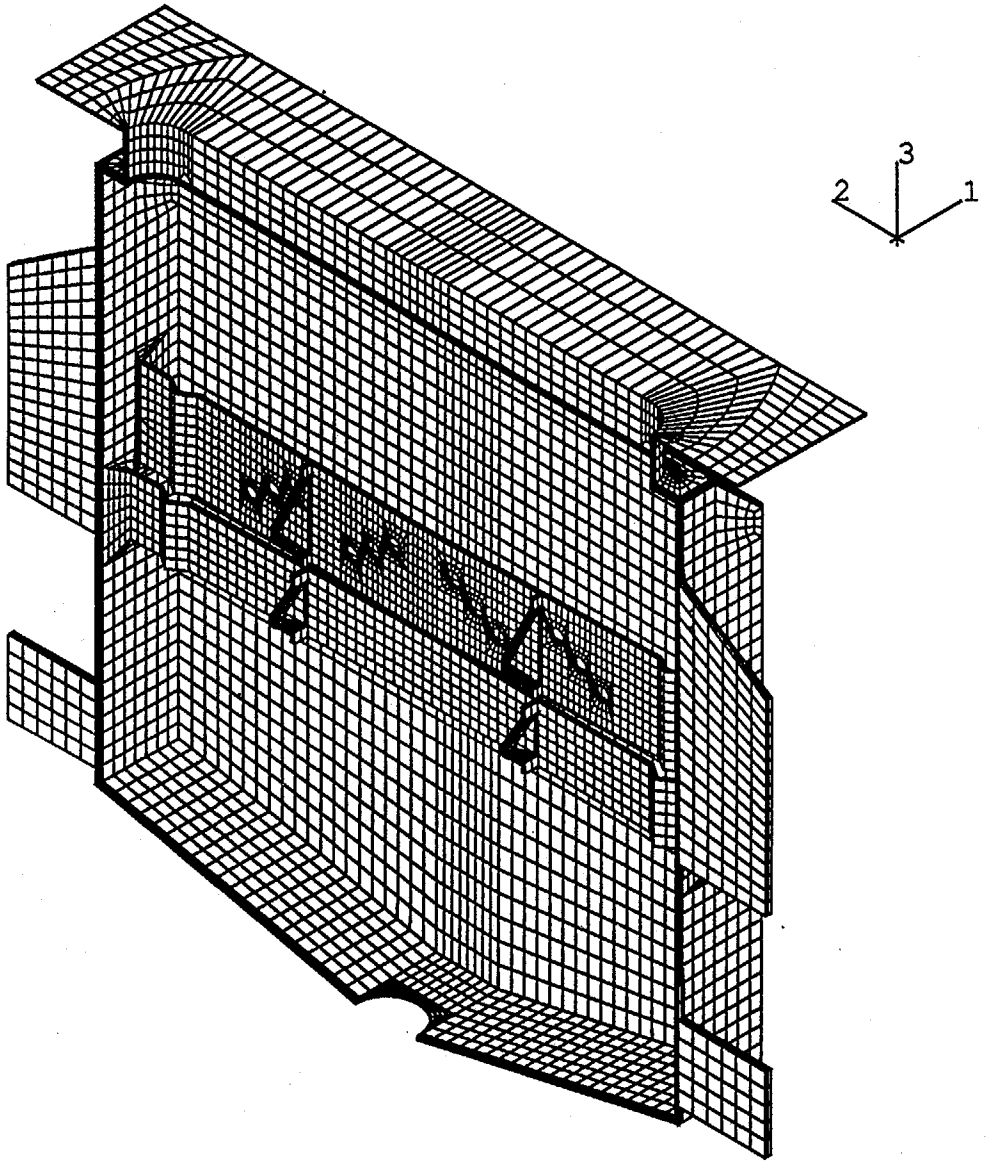

Figure 4-1. Americium/Curium Vitrification Bushing Melter 2A
Finite Element Analysis Mesh

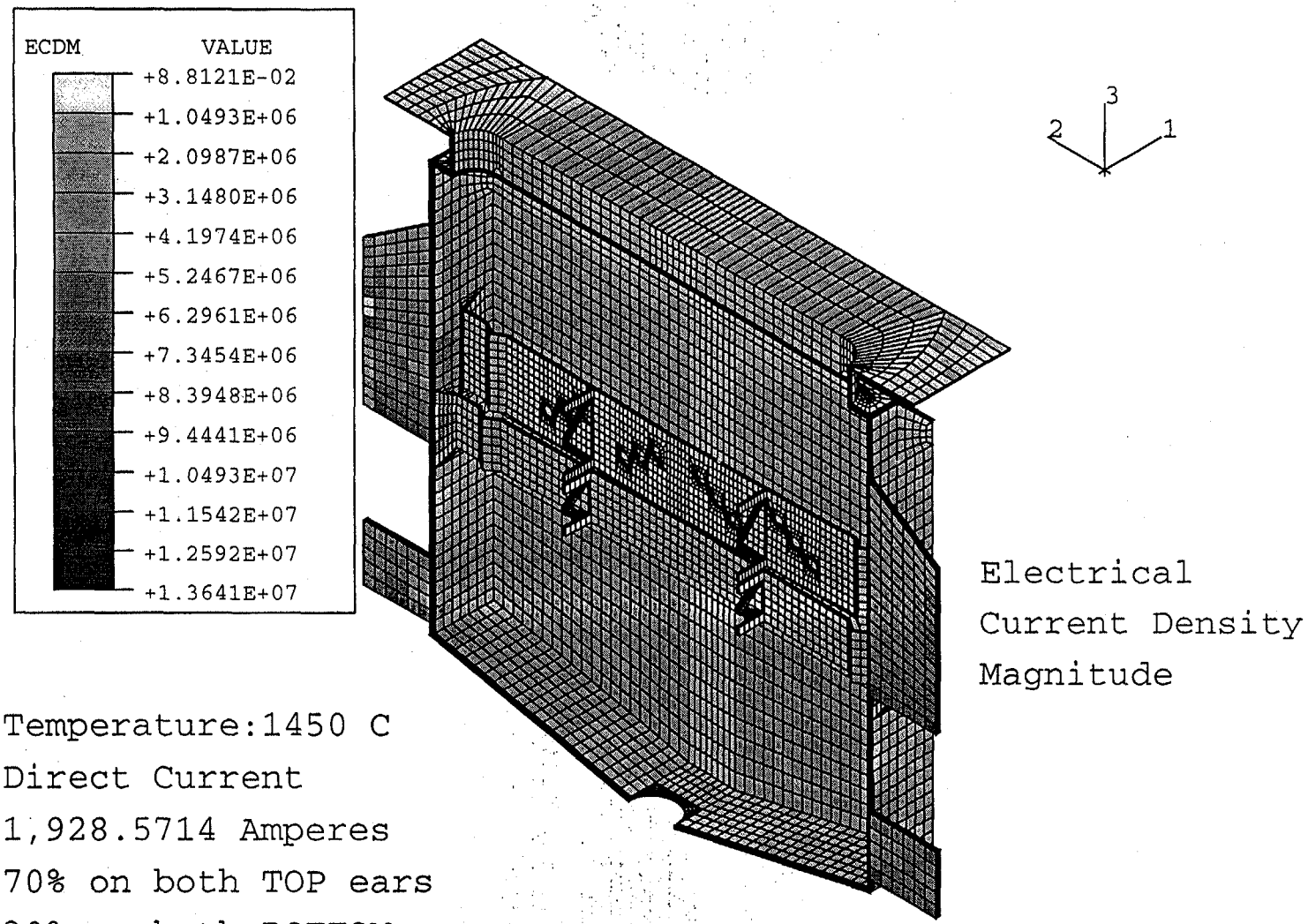

Figure 7-1. Americium/Curium Vitrification Bushing Melter 2A
Current input: 70% on Top Ears, 30% on Bottom Ears
Electrical Current Density Magnitude

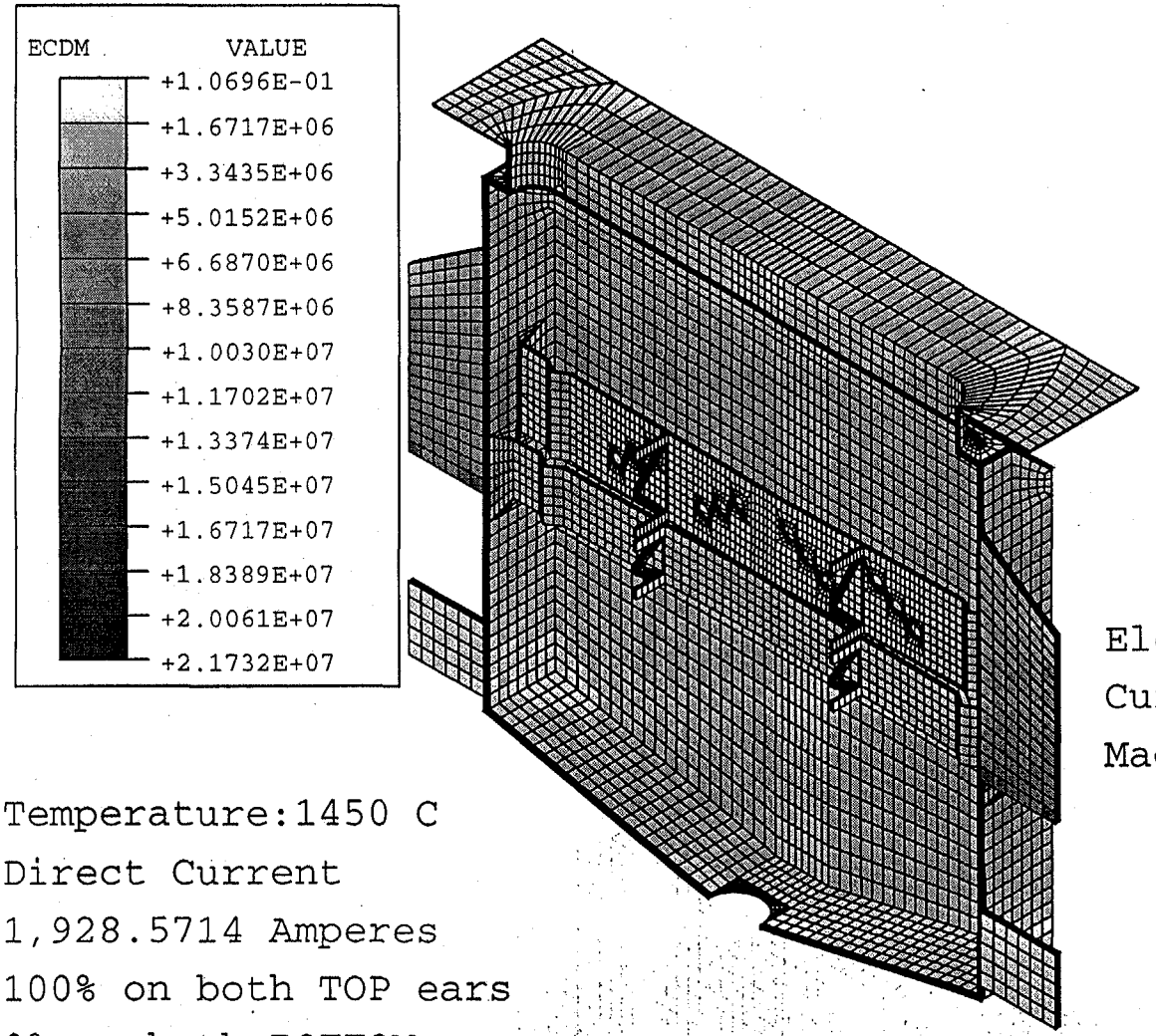

Figure 7-2. Americium/Curium Vitrification Bushing Melter 2A
Current input: 100% on Top Ears, 0% on Bottom Ears
Electrical Current Density Magnitude

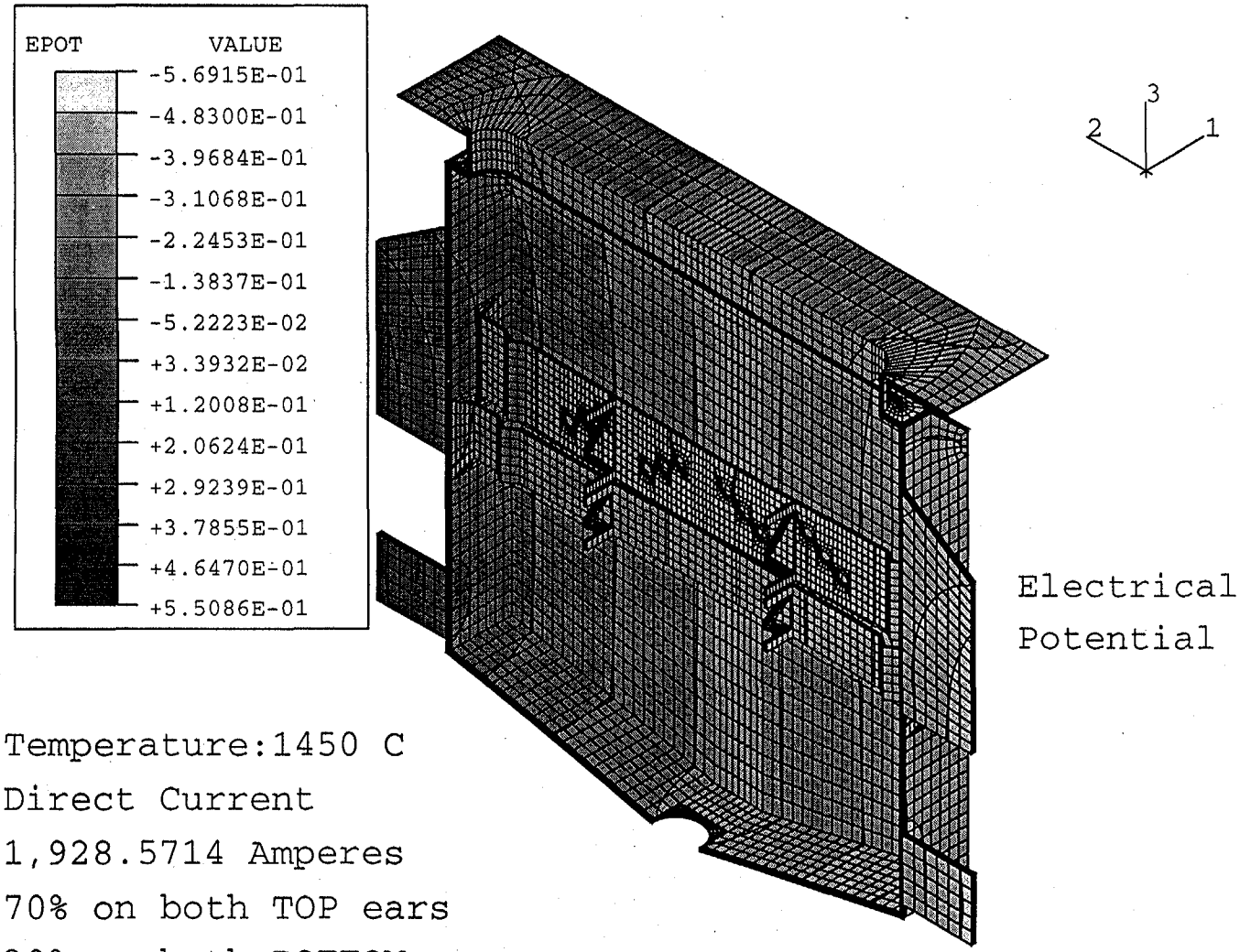

Figure 7-3. Americium/Curium Vitrification Bushing Melter 2A
Current input: 70% on Top Ears, 30% on Bottom Ears
Electrical Potential

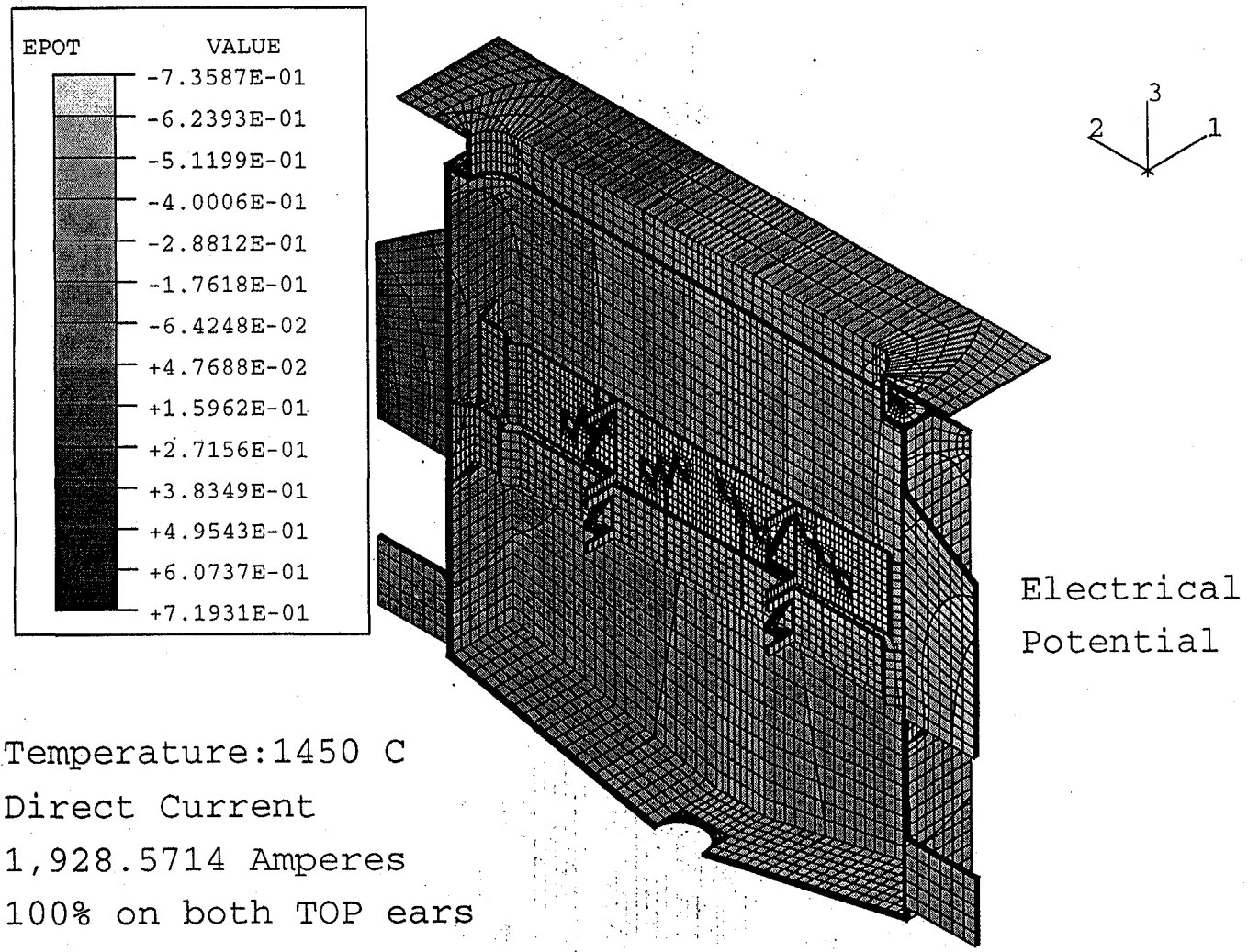

Figure 7-4. Americium/Curium Vitrification Bushing Melter 2A
Current input: 100% on Top Ears, 0% on Bottom Ears
Electrical Potential

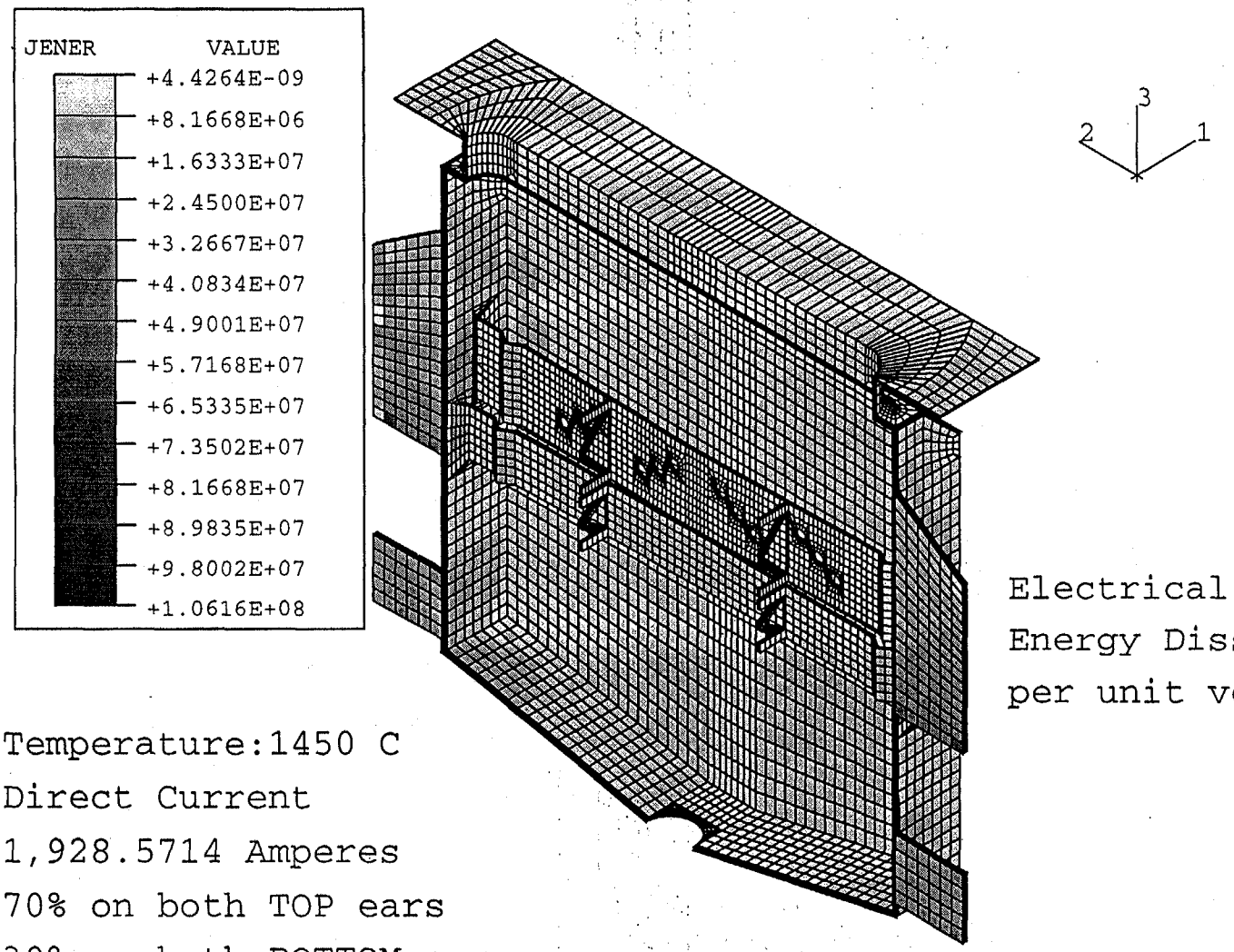

Figure 7-5. Americium/Curium Vitrification Bushing Melter 2A
Current input: 70% on Top Ears, 30% on Bottom Ears
Electrical Energy Dissipated per unit volume

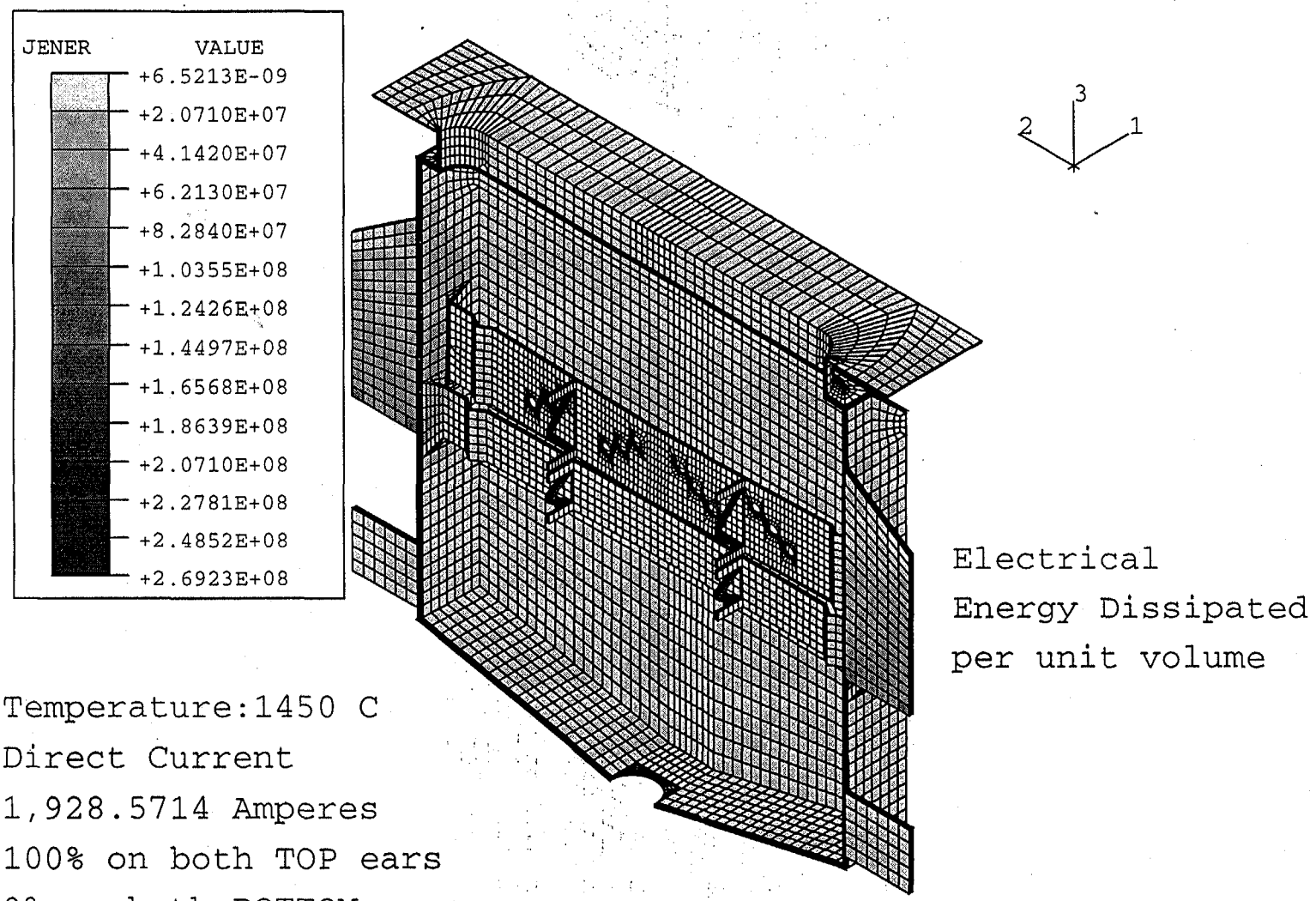

Figure 7-6. Americium/Curium Vitrification Bushing Melter 2A
Current input: 100% on Top Ears, 0% on Bottom Ears
Electrical Energy Dissipated per unit volume

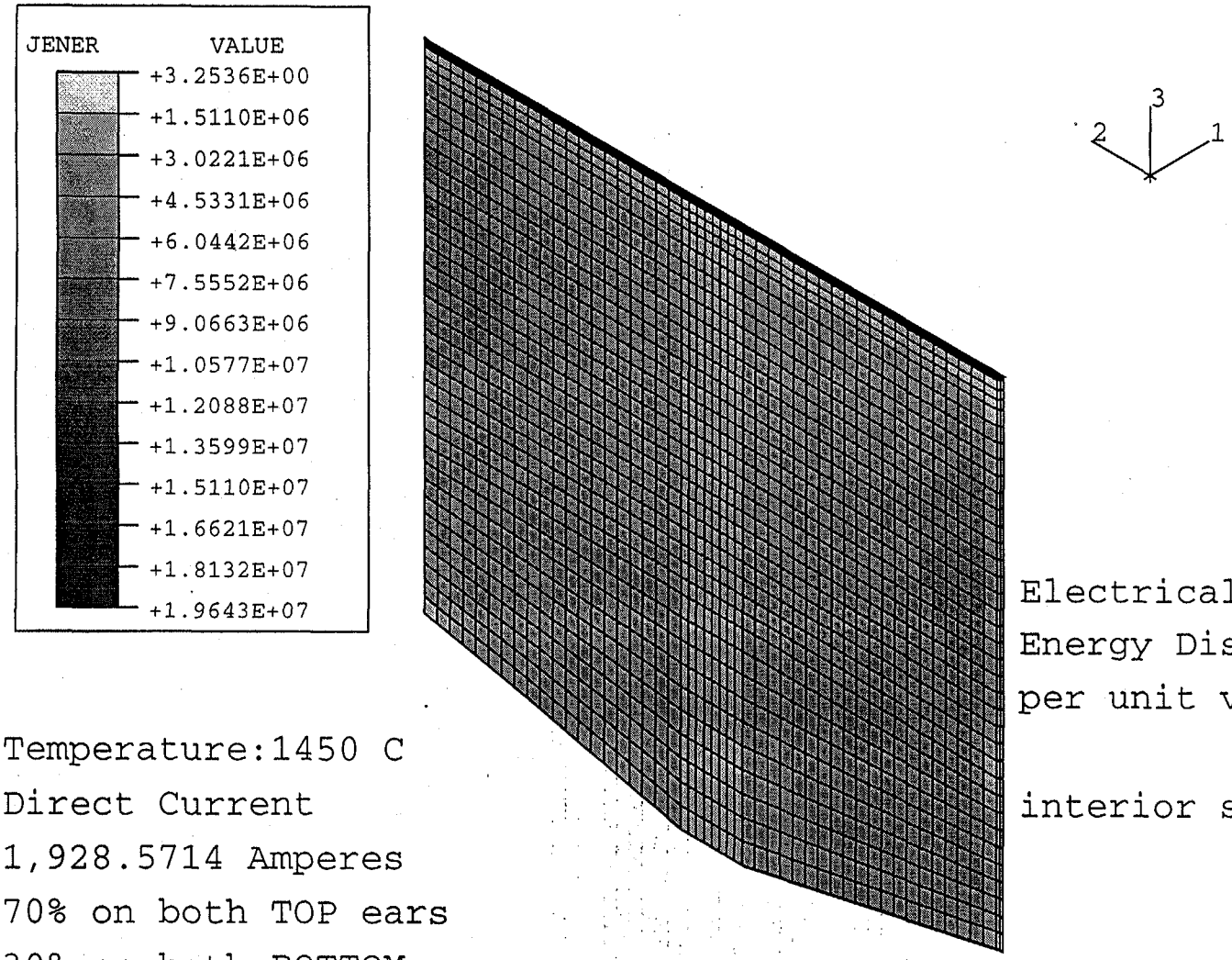

Figure 7-7. Americium/Curium Vitrification Bushing Melter 2A
Current input: 70% on Top Ears, 30% on Bottom Ears
Electrical Energy Dissipated per unit volume in Large Plate

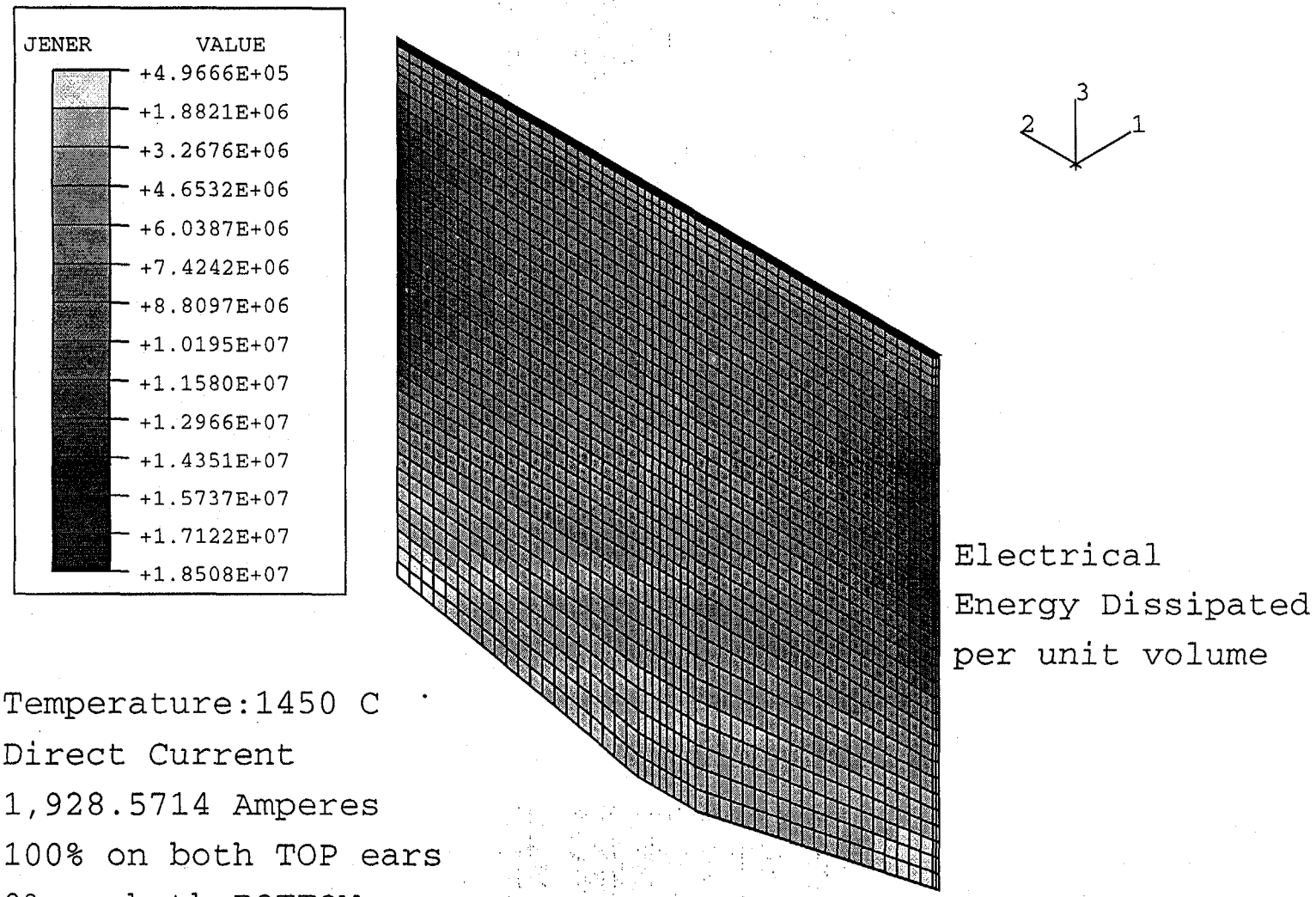

Figure 7-8. Americium/Curium Vitrification Bushing Melter 2A
Current input: 100% on Top Ears, 0% on Bottom Ears
Electrical Energy Dissipated per unit volume in Large Plate

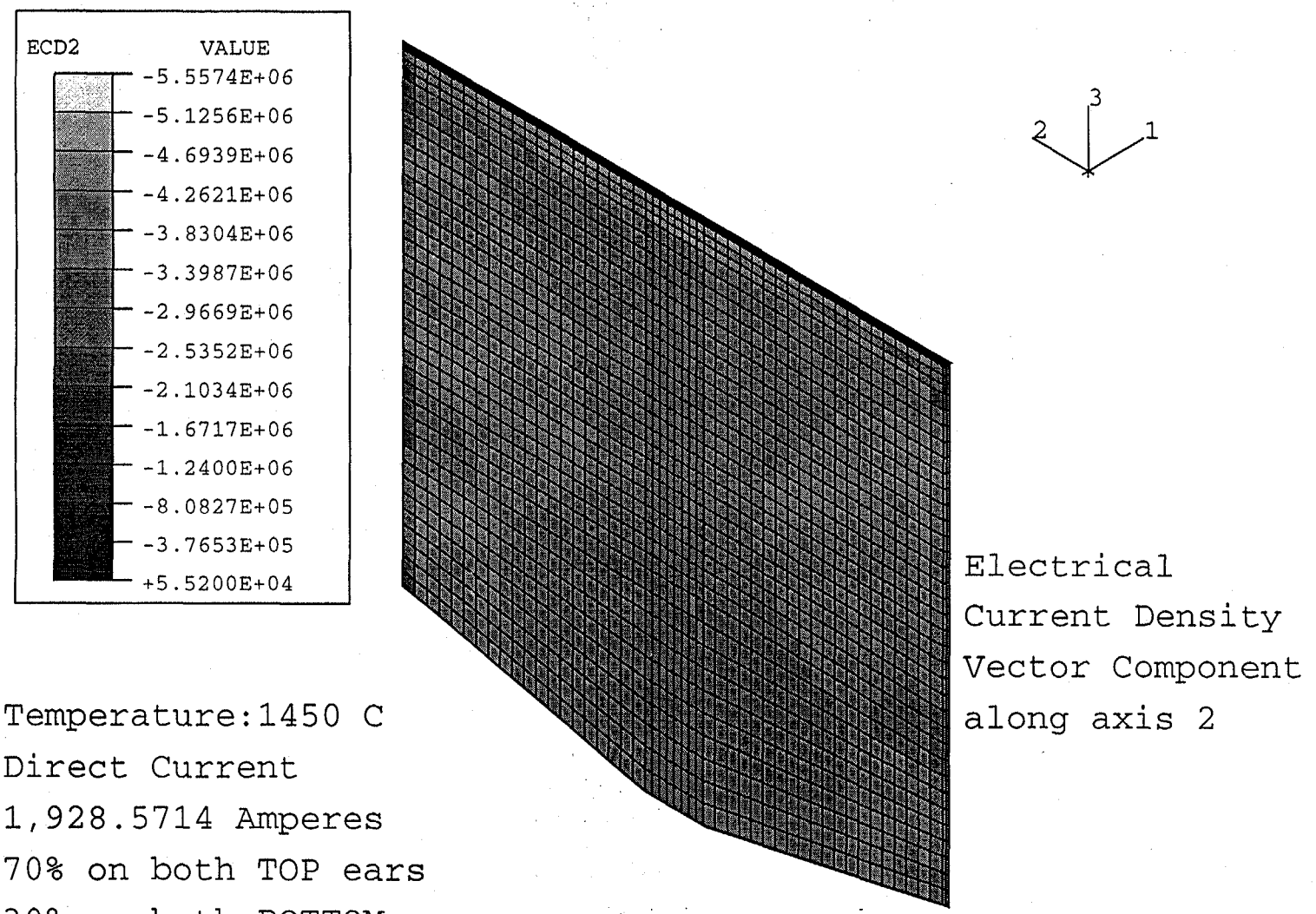

Figure 7-9. Americium/Curium Vitrification Bushing Melter 2A
Current input: 70% on Top Ears, 30% on Bottom Ears
Electrical Current Density Vector C_2 in Large Plate

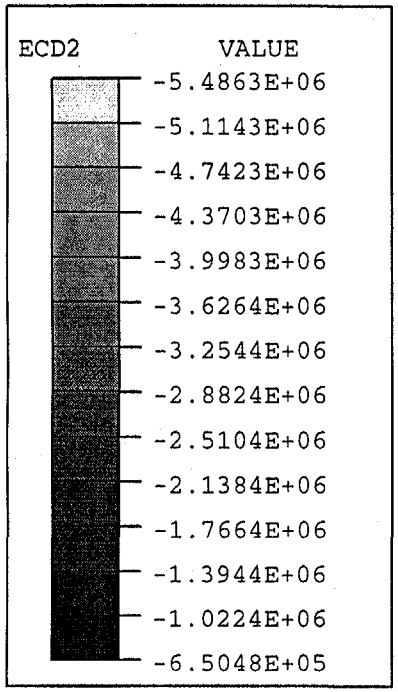

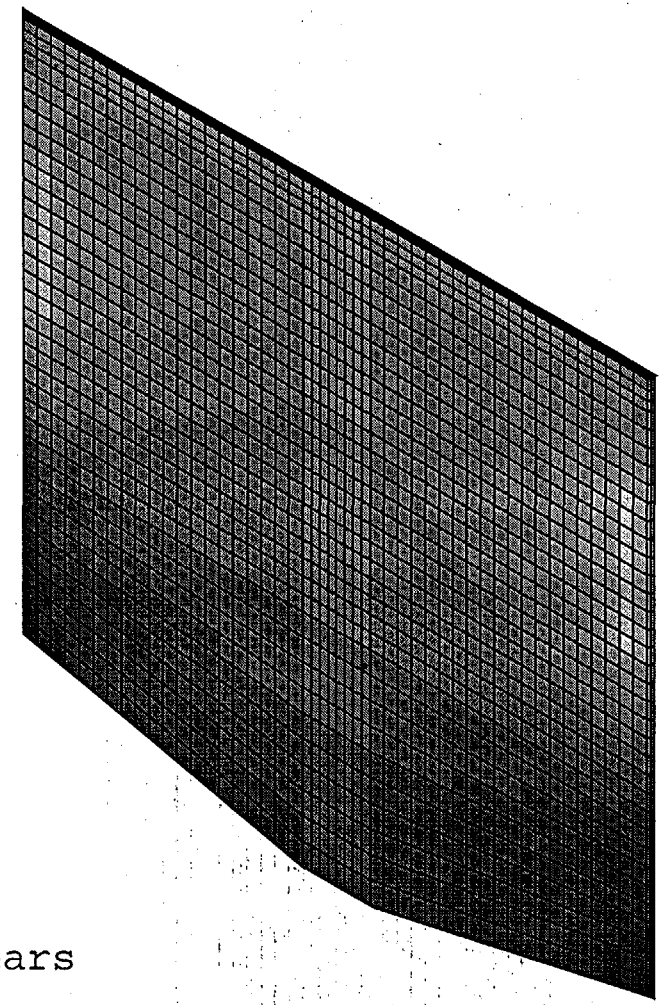

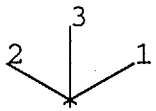

Electrical
Current Density
Vector Component
along axis 2

Temperature:1450 C
Direct Current
1,928.5714 Amperes
100% on both TOP ears
0% on both BOTTOM ears
(without bottom screen)

Figure 7-10. Americium/Curium Vitrification Bushing Melter 2A
Current input: 100% on Top Ears, 0% on Bottom Ears
Electrical Current Density Vector C_2 in Large Plate